HIGH SCHOOL EDITION
Journal of Student Research
Volume 12 Issue 1 (2023)

Trends Among Flux, Luminosity, And Color Indices in High Redshift QSOs

Datta Kurapati[1], Varun Dubagunta[1] and Shyamal Mitra[#]

[1]Leander High School, Leander, TX, USA
[#]Advisor

ABSTRACT

The following study discusses the relationship of high redshift(z) Quasi Stellar Objects'(QSOs) flux, luminosity, and color indices. The paper analyzes observable trends among these 3 variables and uses them to understand the distribution of QSOs across space-time. While many such studies have been conducted in redshift ranges of $1 \leq z \leq 4$, the following research or study has been done in the relatively unexplored date range of $2 \leq z \leq 7$. To answer this question, we used the Sloan Digital Sky Survey to obtain samples, curate the data, and analyze it using Python Data Science tools including Pandas and Matplotlib. The results suggest a general trend of increasing data density with the progression of distance and convergence of QSO Magnitude distributions about the median. This research provides insight into the evolution of QSOs over space-time and why they occurred.

Introduction

Quasi Stellar Objects (QSOs) are starlike extragalactic objects that appear red but are predominantly blue and highly redshifted. The currently accepted scientific model for these bodies is the presence of a supermassive black hole at the center of a galactic nucleus which accretes matter at high velocities, preventing the formation of galactic or stellar structures (Fawcett, V A and Alexander, D M and Rosario, D J and Klindt, L and Lusso, E and Morabito, L K and CalistroRivera, G). This results in high energy output and activity, leading to the production of both luminous and synchrotron radiation. The following study aims to understand the properties of these objects in the range of $2 \leq z \leq 7$. Redshift is a term used to describe the effect of light's wavelength increasing when the distance between it and an object of reference increases. Redshift is a useful measure of distance, since the distance of an extragalactic object from earth is mathematically related to its redshift through the doppler formula, which can also be modified to account for relativistic objects such as QSOs. Furthermore, the farther away an object is, the longer it takes for light to travel that distance, meaning that redshift can also be seen as a measure of time. Magnitude or flux refers to the apparent brightness of an object in the night sky, which is related but not equal to its luminosity or bolometric magnitude, which is its total light output as a body in space. Magnitude and luminosity relationships can be used to derive and predict various trends pertaining to the energetics, distribution, and evolution of astronomical objects. Hence, the study is essential to understand the general distribution of QSOs across significant distances and any changes in their magnitudes over time, and whether these findings convey any evolutionary trend in these objects. Furthermore, the study is essential in affirming the findings of current scientific literature through alternative study methods.

Data

The Sloan Digital Sky Survey (SDSS), an astronomical database compiled from various internationally acclaimed observatories, was used to query for the dataset. The Data Release 7 (DR7), SDDSS's seventh public database release with information pertaining to thousands of astronomical objects, was used in this study as it contained distinct spectroscopic fluxes and redshifts, which are more accurate for faraway objects such as QSOs. The query surveyed the top 100000 QSO samples that were identified spectroscopically, with a description of their spectroscopic redshift(z), spectroscopic flux in each color index, and the Point Spread Function (PSF) magnitude. This method takes multiple frames of the image of a faraway object, centers the image on a single pixel, and distributes this image using a predetermined Gaussian PSF fit. Then, its brightness is adjusted using a nearby star as reference. In this sense, the PSF magnitude is a photometric means of measuring magnitude since it relies on the photographic properties of light to carry out measurement. Spectroscopic flux, inversely, is measured using a spectroscope, which refracts incoming light into a desired number of subjects that can then be assessed individually. The spectroscopic method can be used to better determine redshift and the properties of faraway objects such as QSOs that might be subject to resolution reduction because of distance. In this paper, "flux" will refer to the psf-magnitude of a QSO unless stated otherwise, this is because the spectroscopic flux was used to compute luminosity and therefore, less necessary for analysis. The reason for querying both spectroscopic and photometric flux was to evade any pre-existing relationship between how the data points were observed initially, as this may impact a study of our relationship between flux and luminosity.

Tools and Methods

The data file was processed using Python, with our IDE being Jupyter Notebooks through Visual Studio Code. Using VS Code to run Jupyter Notebook allowed concurrent coding to streamline our work time. Furthermore, libraries such as Pandas, NumPy, and Matplotlib helped us easily analyze data. First, all data rows that were identified as QSOs were selected and the apparent magnitude, which was set as a string in the initial CSV file, was converted to a float so that operations could be performed on it

```
mag0 = data['mag_0'].astype(float)
mag1 = data['mag_1'].astype(float)
mag2 = data['mag_2'].astype(float)
```

Figure 1. Magnitude code

The Relativistic Doppler formula, which modifies the doppler formula to account for fast-moving objects such as QSOs, was used to derive the Radial Velocities of the dataset.

$$V_r = \frac{(1+z)^2 - 1}{(1+z)^2 + 1} * c$$

```
data['V'] = (((((1+z)**2)-1)/(((1+z)**2)+1)) * (3 * (10**5)))
```

Figure 2. Relativistic Doppler Formula in python

Using these values for velocity in Hubble's Law, the distance to each QSO was determined.

$$V = d \text{ x } H$$

```
data['distance'] = data['V']/(69.9)
```

Figure 3. Hubble's Law on python

For this study, it was deemed appropriate to use the lower limit for Hubble's Constant (69.9) as it would indicate the smallest possible distances and by extension, periods in which these QSOs could exist. After obtaining the distances, the distance modulus formula was used to compute the Bolometric Magnitude of all the data points, which can be used to plot the luminosity of QSOs over space. The calculations and code for the distance modulus are shown in the equation below and Figure 4 respectively:

$m - M = 5\log d - 5$

Where m is the apparent magnitude M is the bolometric magnitude, and the *log* is assumed to have a base of 10.

```
data["Abs Mag 0"] = -(-mag0+((5*np.log10(data['distance']*(10**6)))) - 5)
```

Figure 4. Distance Modulus on python

Statistics of the Data Set

The data obtained from the survey was varied and subject to high standard deviation. Therefore, to circumvent this, the data was separated into bins along the x-axis within specific domains of *z*, which were then analyzed for their standard deviation and medians. Then, all values above and below the median that are more than 2 standard deviations away from the mean were removed. This process was then repeated for the newly formed graph to produce a dataset with a clear trend that can then be analyzed for relationships. The following data was collected on each bin for each individual graph:

Table 1. Data for Graph 1: Absolute Magnitude (Luminosity) v Redshift in g. Slope Formula for Line: y = -27.1129 + 1.4731x

Z Interval	Standard Deviation	Median Absolute Magnitude(M)	Mean Absolute Magnitude(M)	Median Redshift (z)	Mean Redshift (z)
Bin 1 ($2 \leq z \leq 3$)	0.694	-23.803	-23.829	2.240	2.33
Bin 2 ($3 < z \leq 4$)	0.603	-23.114	-23.182	3.326	3.395
Bin 3 ($4 < z \leq 5$)	0.786	-22.6246	-22.604	4.30516	4.351
Bin 4 ($5 < z \leq 6$)	1.387	-21.628	-21.974	4.30516	4.351

Table 2. Data for Graph 2: Absolute Magnitude (Luminosity) v Redshift in r. Slope Formula for Line: y = -25.4106 + 0.6907x

Z Interval	Standard Deviation	Median Absolute Magnitude(M)	Mean Absolute Magnitude(M)	Median Redshift (z)	Mean Redshift (z)
Bin 1 ($2 \leq z \leq 3$)	0.694	-23.803	-23.829	2.240	2.33
Bin 2	0.603	-23.114	-23.182	3.326	3.395

(3 < z ≤ 4)					
Bin 3 (4 < z ≤ 5)	0.786	-22.625	-22.604	4.305	4.351
Bin 4 (5 < z ≤ 6)	1.387	-21.628	-21.974	4.305	4.351

Table 3. Data for Graph 3: Absolute Magnitude (Luminosity) v Redshift in i. Slope Formula for Line: M = -24.2495 + 0.2308z

Z interval	Standard Deviation in z	Median Absolute Magnitude(M)	Mean Absolute Magnitude(M)	Median Redshift (z)	Mean Redshift (z)
Bin 1 (2 ≤ z ≤ 3)	0.814	-23.678	-23.682	2.239	2.33
Bin 2 (3 < z ≤ 4)	0.577	-23.246	-23.317	3.326	3.395
Bin 3 (4 < z ≤ 5)	0.535	-23.215	-23.248	4.305	4.35
Bin 4 (5 < z ≤ 6)	0.737	-23.140	-23.187	5.292	5.334

Analysis

The resulting luminosity of the QSOs were then plotted against redshift. This graph was created for all color indices, which are the individually refracted colors obtained from white light coming from the QSOs. Any variations between these metrics would indicate specifics regarding the energetics of the QSO. The g range refers to the color green, while r refers to red, and i refers to infrared. These are the color indices predetermined by the SDSS authors to convey information and The data trend, shown in figures 5, 6, and 7, while scattered at the lower and upper bounds, indicates a general decrease in magnitude as the z approaches 2, indicating that QSOs have been getting brighter at closer distances. An important thing to note is that while the data might be getting scarcer at farther distances, this is not an actual representation of QSO distribution, but rather a limitation of our available observational data at these distances. As for color-specific trends, the calculated luminosity in the g range appears to shift more noticeably than the r or i ranges. This could likely be a result of high energy light being easier to observe, but also a general increase in the luminosity of QSOs as they get closer. The trends seem much more stable across the r and i bands, indicating that light detection capabilities might have not been a limitation. These ranges are the color filters that the quasars were detected at. Red is represented by r, green is represented by green, and the infrared quasars are represented by i. The colors on the graphs below are simply a representation of the color of the filter.

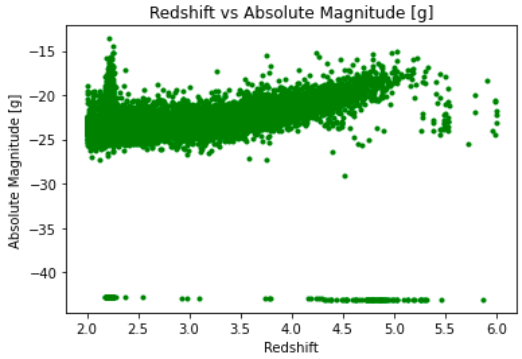

Figure 5. Absolute Magnitude (Luminosity) v Redshift in g

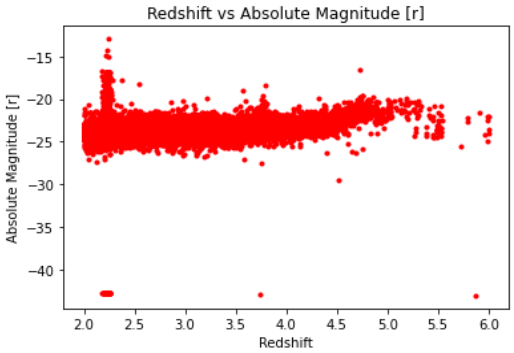

Figure 6. Absolute Magnitude (Luminosity) v Redshift in r

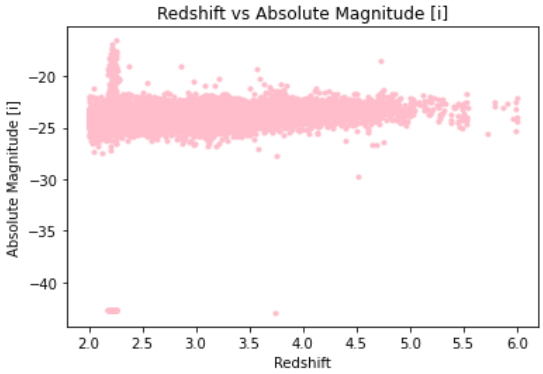

Figure 7. Absolute Magnitude (Luminosity) v Redshift in i

However, the outliers (especially at the minimum range) reduced the scope of the graph and made it difficult to ascertain a trend within the data-dense regions. To remedy this, the data was divided into bins of varying domains depending on the density of data in the region. Then, the median luminosity and standard deviation of each bin were calculated, and all values 2 standard deviations away from the median were removed. The corrected graph is shown in figure 8 below.

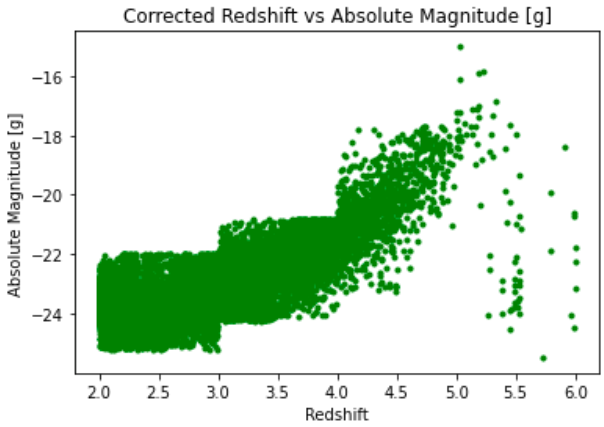

Figure 8. Corrected Absolute Magnitude (Luminosity) v Redshift in g

For each bin, the domain of redshift values were chosen depending on the data density of the region, meaning that the bins get larger as z increases. This was done to account for the scarcity of data at the high redshifts of $5 \leq z \leq 7$. A limitation of this method was the retainment of outliers in the farther ranges since they have a smaller range of values at the median. An interesting outcome of this process was when it was repeated for the r and i graphs (shown in figures 9 and 10), which produced a very similar trend only for the r band:

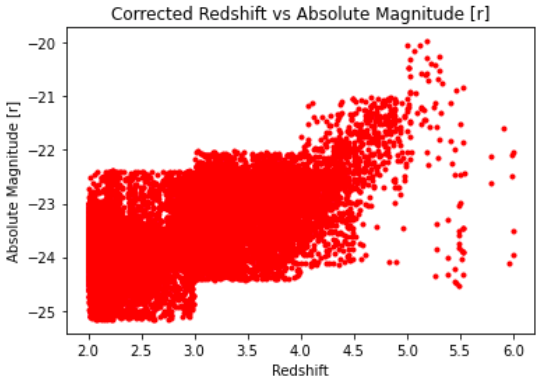

Figure 9. Corrected Absolute Magnitude (Luminosity) v Redshift in r

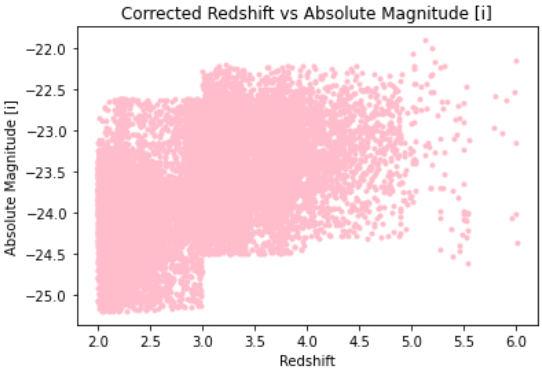

Figure 10. Corrected Absolute Magnitude (Luminosity) v Redshift in i

While the similarities between the curves in the corrected graphs for g and r bands are similar, the i band is much more stable, with a high data density about the median at all redshifts. This could support the theory that QSOs have become more energetic since all bands of luminosities get brighter as redshift decreases, which is corroborated by the relative increase in the rate of change of luminosity as the energy band of the data

points increases. To quantify the subtle variations among the various color indices, best-fit lines were produced for each color index using the medians of each graph as points of reference. These graphs are displayed in figures 14, 15, and 16 below:

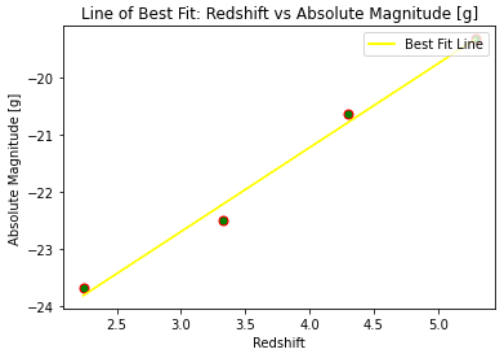

Figure 14. Line of Best Fit for Absolute Magnitude (Luminosity) v Redshift in g. *y = -27.1129 + 1.4731x*

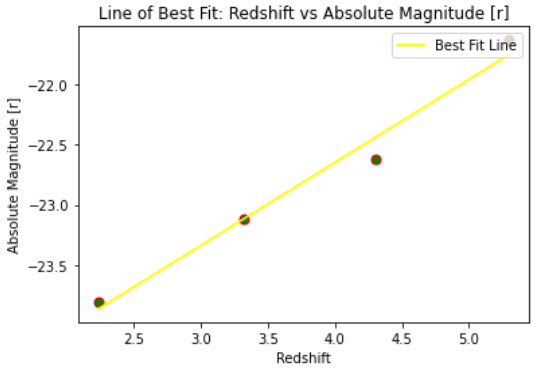

Figure 15. Line of Best Fit for Absolute Magnitude (Luminosity) v Redshift in r. *L = -25.4106 + 0.6907z*

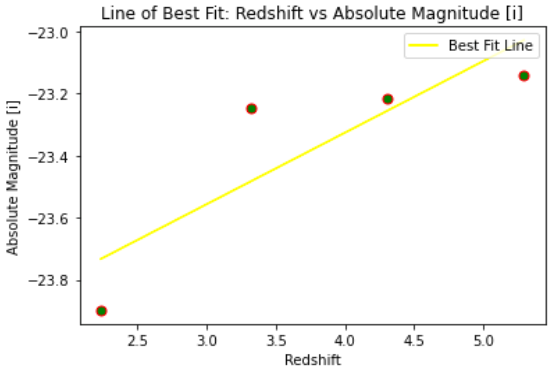

Figure 16. Line of Best Fit for Absolute Magnitude (Luminosity)(L) v Redshift(z) in i. *L = -24.2495 + 0.2308z*

The data points for both g and r have relatively close distribution to the line of best fit, while the i graph shows great variation. The path of the data points indicates more of a gaussian fit as opposed to linear but has not been shown in the interest of indicating the difference in the linearity of the data points.

An unexpected trend during this study was the similarity between graphs of photometric flux and luminosities of the QSOs. The luminosities were gathered using spectroscopic flux and redshift, while the flux values used in the graph were photometric, meaning that the method of data gathering has no bearing on the

trend observed here and that both values are individually observed. To explore this further, the photometric flux of the QSOs was plotted against their Luminosities, which produced a resoundingly linear trend, shown in figures 17,18, and 19. Due to the sample size of the study and low standard deviation in the apparent magnitude across the Absolute Magnitude axis, the following finding can be used to generalize a relationship between the flux and luminosity of QSOs independent of other distance-determining measures, meaning that they have potential use as distance indicators at far distances. This trend is very consistent across all color bands:

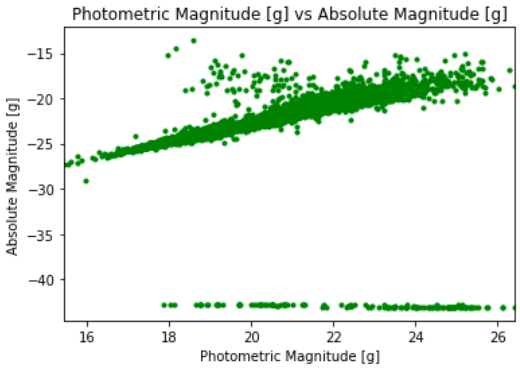

Figure 17. Luminosity v PSF flux in g

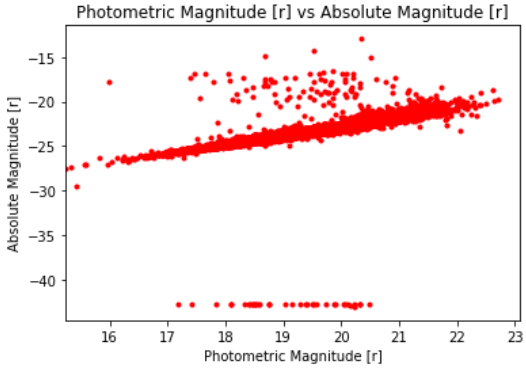

Figure 18. Luminosity v PSF flux in r

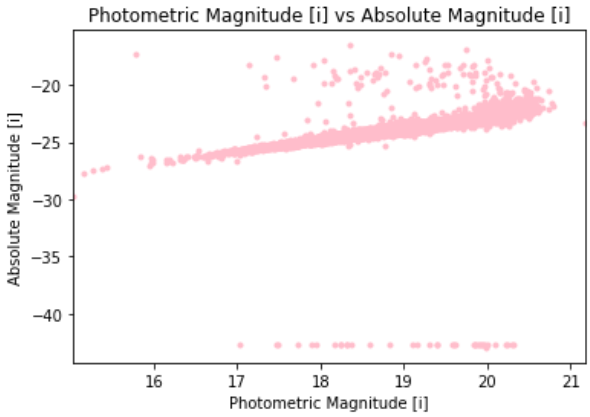

Figure 19. Luminosity v PSF flux in i

The graphs were then corrected using the process of removing outliers by removing all points two standard deviations away from the mean. The corrected data for each color index can be seen in the figures 20, 21, and 22:

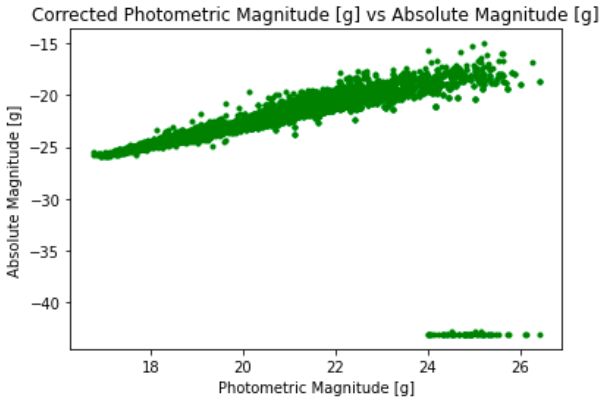

Figure 20. Luminosity v PSF flux in g

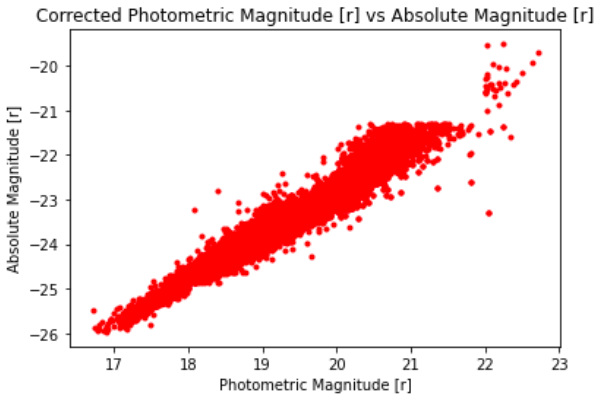

Figure 21. Luminosity v PSF flux in r

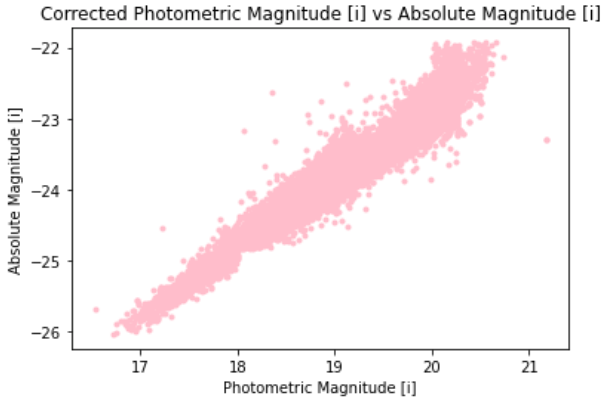

Figure 22. Luminosity v PSF flux in i

The respective lines of best fit have also been presented in the order in figures 23, 24, and 25:

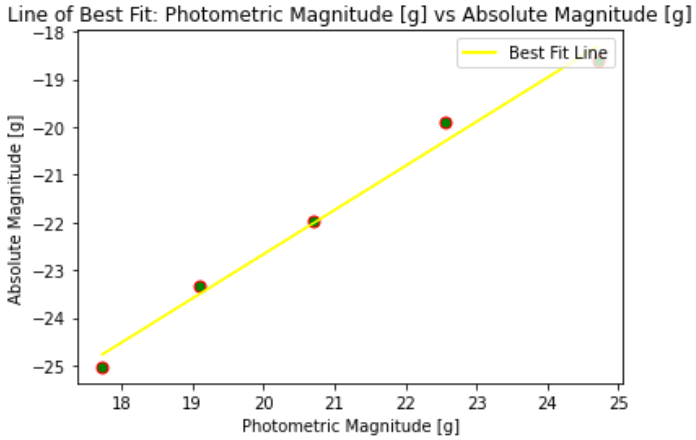

Figure 23. Line of Best Fit for Luminosity(L) v PSF flux(m) in g. *L = -41.2101 + 0.9269m*

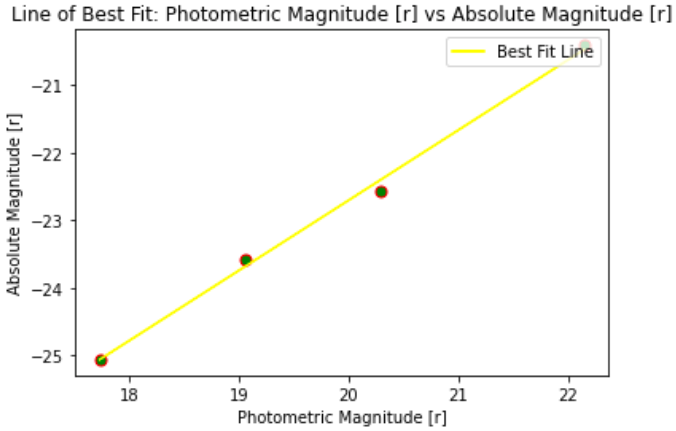

Figure 24. Line of Best Fit for Luminosity(L) v PSF flux(m) in r. *L = -43.4972 + 1.0395m*

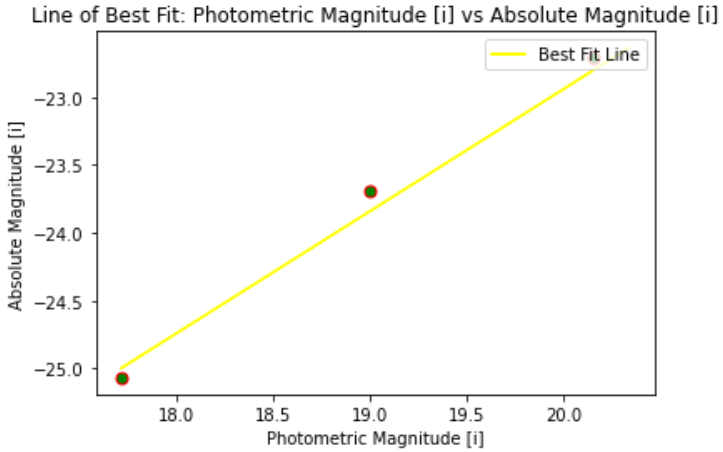

Figure 25. Line of Best Fit for Luminosity(L) v PSF flux(m) in i. $L = -40.8997 + 0.8979m$

The above lines of best fit are well aligned with the data points and indicate a potential for a parametric relation between photometric flux and luminosity. Furthermore, the uniformity of this relationship across all energy filters supports the hypothesis that the flux-luminosity relationship of QSOs is not limited to a specific energy range and is a generalized relationship.

Inferences and Reflection

The results strongly suggest that QSOs at smaller redshifts, i.e., closer to earth are increasing in magnitude, even though the maximum and minimum values are scattered across farther redshifts. This is expected since the brightest QSOs are naturally the most visible at farther distances. However, the trend contradicts this notion and poses important questions regarding the evolution of QSO energy output and what could have caused this trend. The trend demonstrates the ability to be able to use photometric magnitude to be able to find the absolute magnitude of the quasar. A similar result was found by Chen, Shan, and Zhang in their study, "2Mass Observation of Infrared Quasars," where they found that the majority of quasars are between the ranges of 0.3 to 2 in redshift and have the property of an increasing luminosity with a greater redshift. Their study concludes that most of the luminosity emitted by quasars occurs near the infrared bands (Chenm, Shan, & Zhang, 2006). The results are consistent with what we found and help develop the cases for the use of quasars as standard candles over a distance. Additionally, in the study, "Ultra luminous high-redshift quasars from SkyMapper – II. New quasars and the bright end of the luminosity function," by Onken et al. concluded that quasars are extremely luminous at high redshifts (Onken et al., 2022). For future reference, this study could have benefitted from examining more variables and fluxes obtained from other sources, to compare more than 2 methodologies. Perhaps a future study can explore luminosity values derived from more than one set of redshift and flux readings. This study would also likely compare the sizes of QSOs over time and determine if any trend exists between the radius and light output of a QSO. Additionally, analyzing other lines of best fit may have allowed for a more accurate representation of the trends present.

Acknowledgments

The team of this study would like to formally thank Dr. Shyamal Mitra and the UT Austin HSRA program for the guidance and resources to complete this study.

References

K. N. Abazajian, J. K. Adelman-McCarthy, M. A. Agüeros, et al., The Seventh Data Release of the Sloan Digital Sky Survey, *Astrophysical Journal Supplement 182* (2009) 543-558.

Greenstein, J. L., and Schmidt, M. 1964, *The Quasi-Stellar Radio Sources 3C 48 and 3C 273*, Ap. J., 140 1

Hartwick, F. D. A. and Schade, D. 1990, *The Space Distribution of Quasars*, Annual Review of Astronomy and Astrophysics, 28 (1). pp. 437-489

Gupta, R. P. (2022). Constraining variability of coupling constants with bright and extreme quasars. Monthly Notices of the Royal Astronomical Society. https://doi.org/10.1093/mnras/stac1203

Fawcett, V A and Alexander, D M and Rosario, D J and Klindt, L and Lusso, E and Morabito, L K and CalistroRivera, G (2022) 'Fundamental differences in the properties of red and blue quasars: measuring the reddening and accretion properties with X-shooter.', Monthly Notices of the Royal Astronomical Society, 513 (1). pp. 1254-1274.

Chen, P.-S., Shan, H.-G., Zhang, P., & Gao, Y.-F. (2006). 2Mass observation of infrared quasars. Astrophysics and Space Science, 302(1-4), 17-25. https://doi.org/10.1007/s10509-005-9000-0

Onken, C. A., Wolf, C., Bian, F., Fan, X., Hon, W. J., Raithel, D., Tisserand, P., & Lai, S. (2022). Ultraluminous high-redshift quasars from skymapper – II. new quasars and the bright end of the luminosity function. Monthly Notices of the Royal Astronomical Society, 511(1), 572-594. https://doi.org/10.1093/mnras/stac051